Determination of the Phase Boundary of High Molecular Weight Polymer Blends

A. A. Lefebvre,[†] N. P. Balsara,*[,†,‡] J. H. Lee,[†] and C. Vaidyanathan[§]

Department of Chemical Engineering, University of California, Berkeley, California 94720; Materials Sciences Division, Lawrence Berkeley National Laboratory, University of California, Berkeley, California 94720; and Department of Chemical Engineering, Chemistry and Materials Science, Polytechnic University, Six Metrotech Center, Brooklyn, New York 11201

Received April 8, 2002

ABSTRACT: The Flory−Huggins interaction parameter, χ, of an off-critical poly(methylbutylene)/poly(ethylbutylene) blend was measured over a wide temperature (T) and pressure (P) range by comparing small-angle neutron scattering (SANS) profiles from single-phase systems with predictions based on the random phase approximation (RPA). We show that χ, which is a nonlinear function of $1/T$ at low pressures, becomes a linear function of $1/T$ at elevated pressures (above 2.5 kbar). The pressure dependence of the phase boundary (i.e., binodal temperature) of our blend was determined from a series of dissolution experiments wherein a phase-separated sample was heated under isobaric conditions until the SANS profiles were identical to calculations based on the RPA. The binodal, thus obtained, was in quantitative agreement with that computed using the Flory−Huggins theory. The agreement was obtained without any adjustable parameters. Binodals determined by the more traditional cloud point measurements are erroneous due to the presence of large nucleation barriers.

Introduction

Diverse phenomena such as boiling, crystallization, and liquid−liquid phase separation are initiated by nucleation.[1−3] In most systems, the processes that occur during the initial stages of nucleation have escaped experimental scrutiny. Polymeric systems may be considered as model materials for studying the initial stages of nucleation because chain entanglement leads to slow diffusion, which, in turn, enables time-resolved measurements. This paper is part of a series on the subject of nucleation during liquid−liquid phase separation in polymer blends.[4−7] Direct measurements of length and time scales involved in the initial stages of nucleation are reported in refs 4−6. As expected, these length and time scales are strong functions of quench depth, i.e., "distance" from the phase boundary. Unfortunately, the very feature that enables precise measurements of the nonequilibrium processes during nucleation—slow diffusion—hinders the determination of equilibrium properties such as the location of the phase boundary. The main purpose of this paper is to demonstrate a methodology for obtaining the phase boundary of high molecular weight polymer blends.

The most common experiment used for locating the phase boundary in polymer blends is cloud point measurements. In these experiments, a single-phase sample is quenched in a series of steps close to and into the two-phase region. The sample is usually monitored using light scattering, but similar information can be obtained using small-angle neutron scattering (SANS) or small-angle X-ray scattering. The formation of two phases is usually detected when the characteristic length of the phase-separated domains is comparable to the reciprocal of the magnitude of the accessible scattering vector.

Liquid−liquid phase separation is a classic example of a first-order phase transition (except at the critical point) and thus subject to nucleation barriers. To relate the phase boundary (or binodal curve) and the cloud point, information about nucleation barriers is required. While recent theoretical work has shed light on this,[8] a quantitative understanding of nucleation barriers in polymer blends undergoing phase separation does not exist. This lack of understanding is either implicitly or explicitly acknowledged in most papers. Howland et al., for example, used cloud point measurements to serve as a guide for phase separation studies without making any attempt at correlating the binodal with the cloud point measurements.[9] In fact, they pointed out that the cloud point is not synonymous with the anticipated binodal. Similar conclusions are reached by Shibayama et al., who showed the consistency between cloud points determined by neutron and light scattering.[10] There are, however, many other studies where the binodal is assumed to be identical to the cloud point.[11−13] Cummings et al. fit their cloud point data to the binodal calculated using the Flory−Huggins theory and thereby obtained the temperature dependence of Flory−Huggins interaction parameter, χ.[11] Maurer et al. noted the lack of correspondence between the cloud point and the binodal but compared their cloud point measurements to the theoretical binodal curve anyway.[13] The relationship between cloud points and equilibrium thermodynamics in polymer blends with hydrogen-bonding interactions (e.g., ref 14) is considerably more complex and outside the scope of the present paper.

In principle, the binodal could also be obtained by studying the "clearing point", i.e., the dissolution temperature. In this case, nuclei of the homogeneous phase must nucleate from the phase-separated structure. Thus, interpretation of the dissolution temperature in terms of equilibrium thermodynamics is subject to the same difficulties that were found when interpreting the cloud point temperatures. While we were unable to find any paper where the binodal in polymer blends was

[†] Department of Chemical Engineering, University of California, Berkeley.
[‡] Lawrence Berkeley National Laboratory, University of California, Berkeley.
[§] Polytechnic University.

10.1021/ma020552x CCC: $22.00
Published on Web 08/29/2002

located by the dissolution method, it has been used effectively to locate binodals of small molecule mixtures and polymer solutions, e.g. ref 15.

The binodal may be interpreted either as the boundary between the single-phase and two-phase systems (as was done in the experiments discussed thus far[9−15]) or as the locus of compositions of coexisting phases. The most convincing determination of binodals in polymer blends is contained in the work of Scheffold et al.,[16] who used the latter interpretation. They started with ca. 1000 nm thick bilayers of two partially miscible pure polymers and studied the time dependence of the composition profiles as equilibrium was approached by interdiffusion. The bilayers were thin enough so that equilibrium could be attained in a reasonable amount of time but thick enough so that finite size effects and surface interactions were unimportant. The binodal locus thus obtained was in agreement with predictions based on the Flory−Huggins theory, with parameters determined from independent neutron scattering experiments. To our knowledge, this is the only paper where the uncertainty of our understanding of nucleation barriers does not interfere with the measurement of the binodal curve.

In this paper we determine the binodal of a blend of high molecular weight polyolefins, poly(methylbutylene) (PMB) and poly(ethylbutylene) (PEB). These are the materials used in the nucleation experiments described in refs 4−6. We demonstrate that the dissolution temperatures of the PMB/PEB blends are in excellent agreement with the binodal temperatures predicted by the Flory−Huggins theory with no adjustable parameters. Our previous experiments on PMB/PEB blends[5,6,17−21] were restricted to pressures up to 1 kbar. In this paper, we have extended the upper pressure limit to 3.10 kbar. At these higher pressures the data reveal trends that are qualitatively different from those reported earlier in refs 17−21.

Theoretical Background

The Flory−Huggins expression for the free energy density of mixing, ΔG_m, for a mixture of two homopolymers labeled 1 and 2 is given by[22−24]

$$\frac{\Delta G_m}{kT} = \frac{\phi_1 \ln \phi_1}{v_1 N_1} + \frac{(1-\phi_1)\ln(1-\phi_1)}{v_2 N_2} + \frac{\chi \phi_1 (1-\phi_1)}{v_0} \quad (1)$$

where k is the Boltzmann constant, N_i is the number of monomer units in polymer chain i, ϕ_i is the volume fraction of polymer i, χ is the Flory−Huggins interaction parameter, v_i is the volume of monomer i, and v_0 is a reference volume, which for this work is equal to 100 Å^3.

The binodal curve, the curve that separates the one-phase and two-phase regions of the phase diagram, for a Flory−Huggins blend is calculated by simultaneously solving the following two equations

$$\ln\left(\frac{\phi_1^{I}}{\phi_1^{II}}\right) + (\phi_1^{II} - \phi_1^{I})(1 - N_1 v_1 / N_2 v_2) + \frac{\chi(T,P) N_1 v_1}{v_0}((1-\phi_1^{I})^2 - (1-\phi_1^{II})^2) = 0 \quad (2)$$

$$\ln\left(\frac{1-\phi_1^{I}}{1-\phi_1^{II}}\right) + (\phi_1^{I} - \phi_1^{II})(1 - N_2 v_2 / N_1 v_1) + \frac{\chi(T,P) N_2 v_2}{v_0}((\phi_1^{I})^2 - (\phi_1^{II})^2) = 0 \quad (3)$$

where ϕ_1^{I} and ϕ_1^{II} are the volume fractions of polymer 1 in the two coexisting phases labeled I and II. To solve eqs 2 and 3 for a binary polymer blend, the temperature and pressure dependence of v_i and χ must be determined.[25]

The temperature and pressure dependence of the monomer volumes, v_i, used in this study was obtained from *PVT* measurements performed by Krishnamoorti.[26] The Tait equation (see eq 4) is used to calculate monomer volumes as both a function of T and P.[27]

$$v_i(P,T) = V_i(0,T)\left[1 - 0.0894 \ln\left(1 + \frac{P}{B_i(T)}\right)\right] \quad (4)$$

where

$$V_i(0,T) = V_{0,i} \exp(A_i T) \quad (5)$$

and

$$B_i(T) = B_{0,i} \exp(-B_{1i} T) \quad (6)$$

$V_{0,i}$, A_i, $B_{0,i}$, and $B_{1,i}$ were determined by fitting eqs 4−6 to experimental data[26] and are listed in Table 1. The *PVT* measurements of Krishnamoorti were conducted between 24 and 276 °C and 0.1 and 2.00 kbar. Monomer volumes outside this range were obtained by extrapolation.

The random phase approximation (RPA) predicts the scattering profiles from a homogeneous blend of two polymers labeled 1 and 2 by the following equation:[28]

$$I(q) = \left(\frac{b_1}{v_1} - \frac{b_2}{v_2}\right)^2 \left(\frac{1}{N_1 v_1 \phi_1 P_1(q)} + \frac{1}{N_2 v_2 (1-\phi_1) P_2(q)} - \frac{2\chi}{v_0}\right)^{-1} \quad (7)$$

where b_i is the neutron scattering length of the monomer in polymer chain i with a monomer volume v_i and P_i is the Debye function of polymer chain i. The Debye function is given by

$$P_i(q) = \frac{2}{x^2}(e^{-x} + x - 1) \quad (8)$$

where $x = q^2 R_{gi}^2$, $R_{gi}^2 = N_i l_i^2/6$, and l_i is the statistical segment length of polymer i. A least-squares fit of eq 7 to the SANS profiles obtained from single-phase PMB/PEB blends gives χ and l_i at a given T and P. Instead of fitting l_{PMB} and l_{PEB} separately, we use literature values of these parameters ($l_{i,ref}$) and correct both parameters by a factor α to minimize the deviation between theory and experiment,

$$l_i(T,P) = \alpha(T,P) l_{i,ref} \quad (9)$$

Table 1. Tait Equation (Eqs 4−6) Parameters for Determining the Temperature and Pressure Dependence of Monomer Volumes

component	$V_{0,i}$ (A^3)	A_i (K^{-1})	$B_{0,i}$ (kbar)	$B_{1,i}$ (K^{-1})
PMB	110.95	6.94×10^{-4}	8.059	5.10×10^{-3}
PEB	132.15	6.91×10^{-4}	7.167	4.93×10^{-3}

Table 2. Characteristics of Polymers

polymer	density (g/cm^3)	av no. of D atoms per 6 C atoms	molec mass (g/mol)	polydispersity index
PMB	0.9192	6.26	1.7×10^5	1.02
PEB	0.8637	0	2.2×10^5	1.08

where $l_{i,\mathrm{ref}}$ is the published statistical segment length at atmospheric temperature and pressure.[29]

Experimental Section

Partially deuterated poly(methylbutylene) (PMB) and hydrogenous poly(ethylbutylene) (PEB) were synthesized and characterized using the methods described in refs 29 and 30. The characteristics of the polymers are given in Table 2. A binary blend of PMB/PEB was made by dissolving the components in cyclohexane and then drying the blend to a constant weight in a vacuum oven at 70 °C. The volume fraction of PMB, ϕ, in the blend used in these experiments was 0.160. We refer to this blend as B3.[31]

Small-angle neutron scattering experiments (SANS) were performed on the NG3 beamline at the National Institute of Standards and Technology (NIST) in Gaithersburg, MD, using the NIST pressure cell. The temperature and pressure range of our experiments were 29 °C $\leq T \leq$ 163 °C and 0.03 kbar $\leq P \leq$ 3.10 kbar. Prior to each experiment the integrity of the sample was verified by measuring the SANS profiles at a convenient temperature and pressure in the one-phase region (106 °C and 0.03 kbar). Excellent overlap of the experimental data was obtained in all cases. We conducted three types of SANS experiments: (1) static experiments wherein the SANS profiles were monitored after step changes in T and P, (2) time-resolved experiments to study phase separation after quenching the sample from the single-phase to the two-phase region, and (3) kinetics experiments to study dissolution wherein the sample was gradually heated from the two-phase to the single-phase region. The instrument configurations used in these studies are given in ref 33. For the static measurements, the time for data acquisition was 5 min, and data acquisition was started 5 min after the cell temperature and pressure had equilibrated. For the dissolution experiments, the data acquisition time was 3 min, while that for the phase separation experiments was 3−30 min (see refs 5 and 33 for details). The scattering data were collected using a 128 × 128 pixel two-dimensional detector, corrected for background scattering, empty cell scattering, and detector sensitivity. All of the scattering profiles were azimuthally symmetric. We thus report the azimuthally averaged scattering intensity as a function of q [$q = 4\pi \sin(\theta/2)/\lambda$, θ is the scattering angle]. The raw data for both the static and dissolution experiments were corrected for background scattering, empty cell scattering, and detector sensitivity and converted to absolute scattering intensity, $I(q)$, using methods and secondary standards described in ref 32. The raw data obtained from the phase separation experiments (λ = 14 Å) were also converted to absolute scattering intensity using a method similar to that described in ref 32. The scaling factor for converting the corrected scattering intensity in the $\lambda = 14$ Å configuration to absolute scattering intensity was obtained by matching the SANS profile of the secondary standard in this configuration to that obtained in the $\lambda = 6$ Å configuration in the range of q values accessible to both configurations.[33]

Results and Discussion

χ Parameter. From previous work on PMB/PEB blends,[17] the binodal temperature of our sample B3 at 0.03 kbar (the lower limit of our P window) was computed to be 70 °C. The sample was heated well above this temperature to 163 °C for 35 min to homogenize the blend. The sample was then cooled in a stepwise manner from 144 to 49 °C in approximately 20 °C steps. At each temperature the pressure was increased in intervals of approximately 0.86 kbar from 0.03 to 3.10 kbar. SANS data were recorded at each temperature and pressure step. We show typical plots of the absolute scattering intensity, I, vs the scattering vector, q, at selected T and P. The solid curves in Figure 1 are the least-squares fit of eq 7 to the data with adjustable parameters χ and α.[34] The other parameters were determined from independent measurements using methods described in refs 29 and 33 and are listed in Table 3. Uniformly good agreement between the experimental data and the theoretical fits is obtained in both the single-phase and metastable regions. Justification for using data from supercooled PMB/PEB blends is given in ref 17. By fitting all of the measured SANS profiles to eq 7, we determined the temperature and pressure dependence of χ and α.

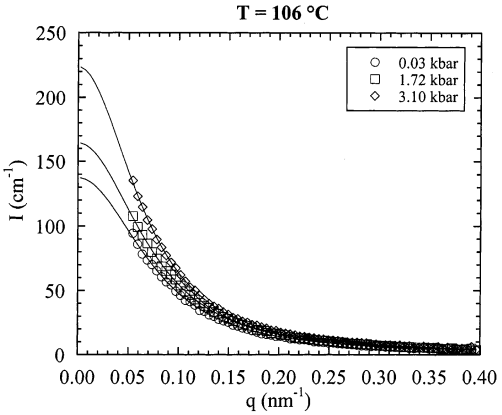

Figure 1. Typical SANS profiles of B3. Scattering intensity, I, vs the scattering vector, q, at 106 °C and selected pressures. The solid curves are the least-squares RPA fits.

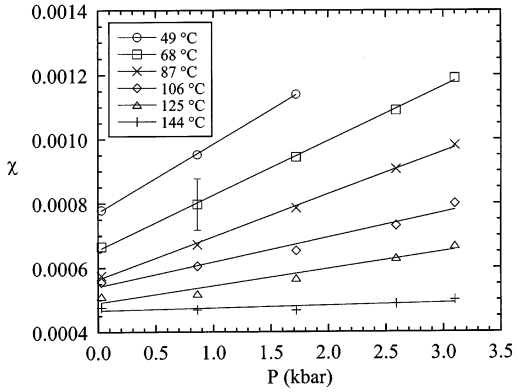

Figure 2. Flory−Huggins interaction parameter, χ, vs P at all temperatures determined from SANS measurements on the B3 blend. The solid lines are least-squares linear fits through the data at each temperature. The error bars indicate the typical uncertainty in χ.[49]

Table 3. Parameters Used for RPA Calculations

parameter	PMB	PEB
N_i	2312	2630
v_i (Å^3/monomer)	136.1	162.0
$l_{i,\mathrm{ref}}$ (Å)	8.26	7.93
b_i (Å)	4.90×10^{-4}	-4.98×10^{-5}

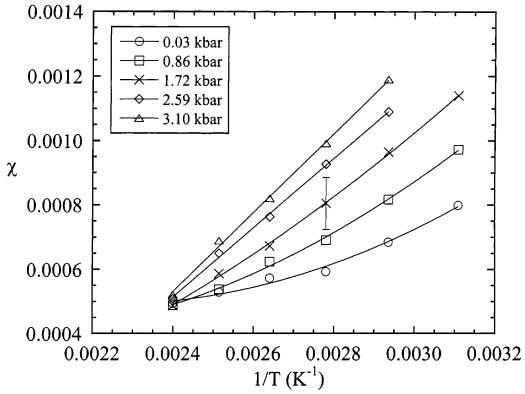

Figure 3. Flory−Huggins interaction parameter, χ, vs $1/T$ at all pressures for the B3 blend. It is evident that the χ dependence on $1/T$ changes from a quadratic dependence at low pressures ($P < 2.59$ kbar) to a linear dependence at higher pressures ($P \geq 2.59$ kbar). The solid lines and curves are least-squares fits through the data. The error bars indicate the typical uncertainty in χ.[49]

A plot of χ vs P at constant T reveals a linear dependence over the entire T and P window (Figure 2). The lines in Figure 2 are least-squares linear fits through the data where

$$\chi(T,P) = D(T) + E(T)P \tag{10}$$

and the temperature-dependent parameters D and E are given in Table 4. In Figure 3 we plot χ vs $1/T$ at selected pressures. For pressures up to 1 kbar, it was shown that the χ parameter between PMB and PEB chains could be approximated by a quadratic function of $1/T$,[17−20,35]

$$\chi(T,P) = A(P) + \frac{B(P)}{T} + \frac{C(P)}{T^2} \tag{11}$$

where A, B, and C are pressure-dependent parameters and are given in Table 5. In contrast, the χ parameter of most polymer blends exhibits a linear dependence on $1/T$.[36,37] The nonlinear $1/T$ dependence is clearly seen in the low-pressure data in Figure 3. At temperatures below 100 °C, the state of PMB/PEB blends is a strong function of $1/T$ while at temperatures above 100 °C, the state of PMB/PEB blends is a weak function of $1/T$. While the molecular origin of this crossover is not known, it is clear that PMB/PEB blends at atmospheric pressure exhibit complexity that is outside the usual approximations of the Flory−Huggins theory. An interesting observation is that, at the two highest pressures, we find a linear dependence of χ on $1/T$. This suggests that the complexity of PMB/PEB blends is pressure-dependent, and better adherence to the Flory−Huggins theory is obtained at higher pressures. This observation may provide a clue about the molecular origin of complex phase behavior in polymer blends. In some studies, it is suggested that the deviations from Flory−Huggins theory are due to specific shapes of the monomers.[38] If this were the case, one would expect increased complexity at elevated pressures when the monomers are forced in close contact. Our observation suggests that the reason for complex thermodynamics in PMB/PEB blends lies elsewhere. This trend toward thermodynamic simplicity at elevated pressures was not evident in our previous study on PMB/PEB blends[17] due to the limited range of the pressure cell used therein. The other features seen in Figures 2 and 3 (e.g., the dramatic decrease in E with increasing temperature) are discussed in detail in ref 17.

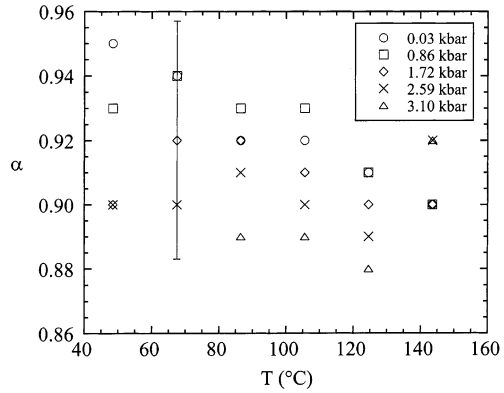

Figure 4. Temperature and pressure dependence of α, the chain expansion/contraction coefficient. The error bars indicate the typical uncertainty in α.[49]

Table 4. Parameters Describing the Pressure Dependence of χ (Eq 10)

temp (°C)	D	E (kbar^{-1})	temp (°C)	D	E (kbar^{-1})
48	7.71×10^{-4}	2.14×10^{-4}	106	5.41×10^{-4}	7.71×10^{-5}
68	6.55×10^{-4}	1.70×10^{-4}	125	4.90×10^{-4}	5.35×10^{-5}
87	5.64×10^{-4}	1.33×10^{-4}	144	4.66×10^{-4}	8.14×10^{-6}

Table 5. Parameters Describing the Temperature Dependence of χ (Eq 11)

press. (kbar)	A	B (K)	C (K^2)
0.03	0.002 46	−1.766	395.69
0.86	0.001 68	−1.405	378.30
1.72	0.000 24	−0.528	262.86
2.59	−0.002 07	1.076	0
3.10	−0.002 41	1.226	0

We show α as a function of T at constant P in Figure 4. The changes in α are unremarkable. The statistical segment lengths in our blend over the entire temperature and pressure window are within 12% of the published value at atmospheric temperature and pressure.

This completes the determination of the parameters needed to compute the binodal for our PMB/PEB blend (eqs 2 and 3). We thus turn to the experimental determination of the binodal.

Binodal. The PMB/PEB blend was stored at atmospheric temperature and pressure for about a week prior to the experiments. The sample was loaded into the pressure cell and heated at a constant pressure of 0.03 kbar from 68 to 163 °C in steps, and $I(q)$ at selected temperatures was measured. The inset of Figure 5 shows typical $I(q)$ obtained during the heating run in the Zimm format: $1/I$ vs q^2 for 0.05 nm^{-1} < q < 0.13 nm^{-1}. The solid lines through the data are least-squares linear fits over the q range shown. Using these fits, we obtain an estimate of I_0, the extrapolated scattering intensity at $q = 0$. In Figure 5 we plot $1/I_0$ vs $1/T$. During the heating run (circles), the value of $1/I_0$ is negative at temperatures below 73 °C. This unphysical result is due to phase separation; the size of the phase-separated domains is well outside the q-window of our SANS experiments.[39] It is clear that the sample was thus in the two-phase region for 1 week (after it was made and before we began the SANS experiments). Despite this, our blend was optically clear. It is evident that optical cloud points cannot be used to determine the binodal in our system.

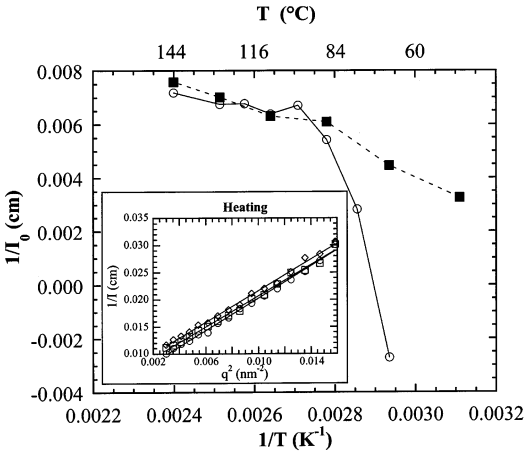

Figure 5. Reciprocal of the absolute scattering intensity extrapolated to $q = 0$, $1/I_0$, vs $1/T$ for the B3 blend during both the heating (circles) and cooling (squares) runs. Inset: inverse of the absolute scattering intensity, $1/I$, vs q^2 at 87 °C (circles), 106 °C (squares), and 144 °C (diamonds) and 0.03 kbar obtained during the heating run. The solid lines are least-squares linear fits through the data that are extrapolated to $q = 0$, thus yielding an estimate $1/I_0$.

In Figure 5 we see that the value of $1/I_0$ increases rapidly upon heating until about 90 °C. Further increase in temperature has a relatively small effect on $1/I_0$. This abrupt change at 90 °C suggests that the sample has crossed the phase boundary and become single phase. After heating the sample well above the phase boundary (up to 163 °C), the sample was cooled in steps, and $I(q)$ was recorded at selected temperatures and pressures.[40] The temperature dependence of $1/I_0$ during the cooling experiment (squares) is also shown in Figure 5. At temperatures above 90 °C, the values of I_0 obtained during the heating and cooling runs are nearly coincident, i.e., independent of history. In contrast, severe hysteresis is seen at temperatures below 90 °C. Hysteresis loops are expected in the vicinity of a first-order phase transition due to the presence of nucleation barriers. In our PMB/PEB blends, the hysteresis curves do not form a closed loop in the temperature window (see Figure 5). This is an indication of the severity of the nucleation barriers in our system. The cooling data in Figure 5 show neither a discontinuity nor a change in slope. It is thus clear that neutron cloud point measurements, which involve cooling the sample from the single-phase region into the two-phase region, cannot be used to locate the binodal in our system. Since both optical and neutron cloud points cannot be used to determine the binodal in our system, we were forced to study the possibility of locating the binodal using dissolution experiments.

The sample was homogenized before each dissolution experiment by heating to 106 °C at 0.03 kbar. The sample was then quenched into the two-phase region and kept there until significant phase separation had taken place. The quench was conducted in two steps: the sample was first cooled under isobaric conditions, at 0.03 kbar, to 58 °C and then subjected to an isothermal pressure quench. The state of the system was monitored throughout the quenching process by SANS. No evidence of phase separation was found after the first quenching step. Time zero ($t = 0$) is thus defined as the time at which the pressure quench (second step) was initiated. In Figure 6 we show $I(q)$ during phase separation for the 2.00 kbar quench. This resulted in a

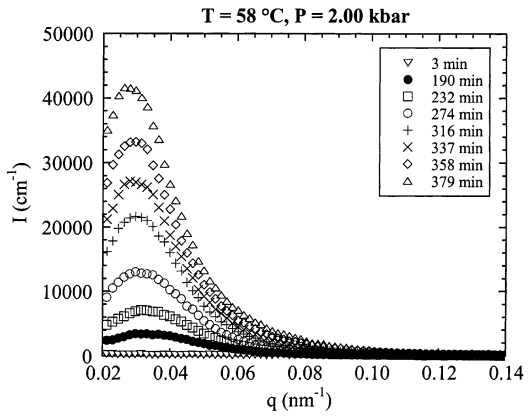

Figure 6. Time dependence of the scattering profiles during the phase separation step at 58 °C and 2.00 kbar.

substantial increase in $I(q)$, as seen in Figure 6. Phase separation was allowed to proceed for 379 min. This completes preparation of the sample for the dissolution experiment.

Dissolution of the phase-separated structure was studied by heating the sample under isobaric conditions in a series of ca. 10 °C steps. Time zero ($t = 0$) for the dissolution experiment is taken to be the time at which the first heating step was initiated. We took five consecutive $I(q)$ scans at each temperature (with 3 min counting intervals). $I(q)$ data obtained during the dissolution experiment at 2.00 kbar at selected temperatures and times are shown in Figure 7a–c. In Figure 7a we show data obtained after the first heating step to 68 °C. We see that increasing the sample temperature from 58 to 68 °C (at constant pressure) arrests phase separation, and $I(q)$ now decreases with time. The curve in Figure 7a is the computed $I(q)$ using RPA and thus represents the expected $I(q)$ for a homogeneous sample. At 18 min, the measured $I(q)$ at low q ($q < 0.05$ nm^{-1}) is an order of magnitude larger than that of the homogeneous sample. It is clear that homogenization of the sample at 68 °C either will not occur at all or will require times that are entirely outside our experimental window. Increasing the sample temperature further results in a decrease in $I(q)$. Data obtained at $t = 79$ min at 96 °C (Figure 7b) are within a factor of 2 of that expected from the homogeneous system. At 106 °C (Figure 7c), we see that the measured $I(q)$ obtained at 95 and 99 min is in quantitative agreement with that expected from the homogeneous system. We thus conclude that the sample is homogeneous at this point.

We conducted four dissolution runs, all starting with a quench from the homogeneous state (106 °C and 0.03 kbar) to 58 °C and pressures indicated in Table 6. The times used for developing the phase-separated structures at different pressures are also given in Table 6. The results of the dissolution experiments are summarized in Figure 8 where we show the scattering intensity at $q = 0.021$ nm^{-1} measured in the fifth (final) time interval at each temperature step $I_F(T)$ normalized by the measured intensity at $q = 0.021$ nm^{-1} in the final time interval at the last temperature $I_F(T_{last})$ of the dissolution experiment $\rho = I_F(T)/I_F(T_{last})$.[41] In one-phase samples $\rho \approx 1$, and the arrows in Figure 8 show the first temperature step that led to $\rho \approx 1$. We define the binodal temperature, T_b, as the midpoint of the temperature step that first leads to $\rho \approx 1$.

In Figure 9 we compare the experimentally determined binodal for our blend in $T-P$ space (symbols) with

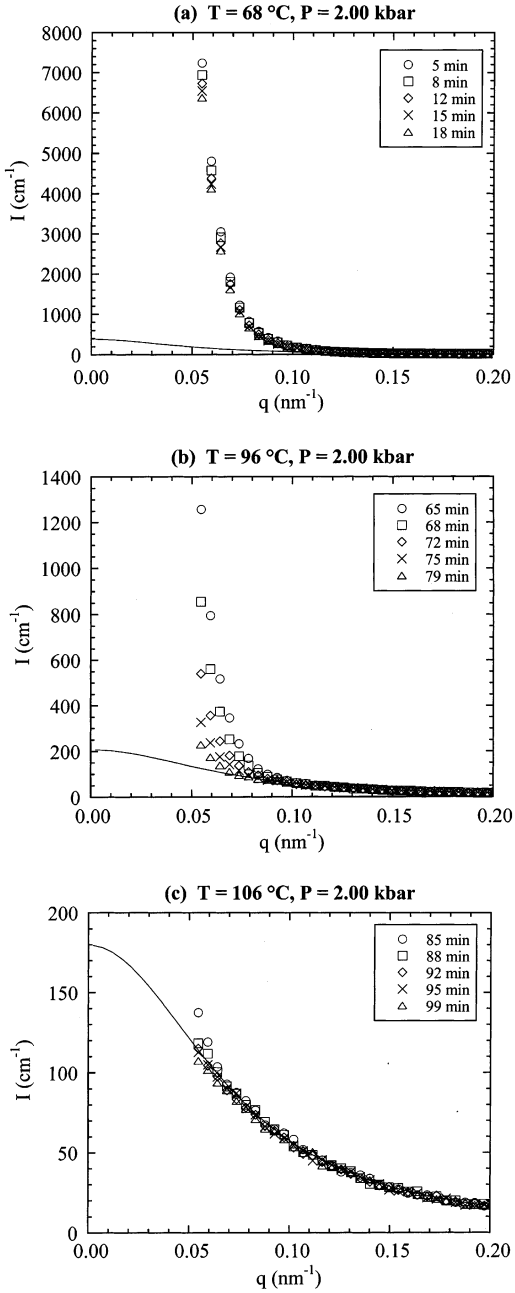

Figure 7. Time dependence of the scattering profiles during the dissolution experiment after phase separation at 58 °C and 2.00 kbar: (a) 68, (b) 96, (c) 106 °C. The curves are RPA predictions (eq 7) using $\chi(T,P)$ given in Figures 2 and 3 and Tables 4 and 5.

Table 6. Sample Preparation for Dissolution Experiments

temp (°C)	press. (kbar)	length of phase separation experiment (min)
58	1.24	945
58	1.66	349
58	2.00	379
58	3.10	328

theoretical predictions. The predictions were obtained by simultaneous solution of equations 2 and 3, to obtain Φ_1^{II} and χ with $\Phi_1^{I} = 0.160$. All other parameters are given by equations 4−6, and Tables 1 and 3. The binodal temperature at a given pressure can then be calculated because χ is a known function of Tan P (Tables 4 and 5). The curve in Figure 9 is the result of these calculations. The agreement between theory and experiment

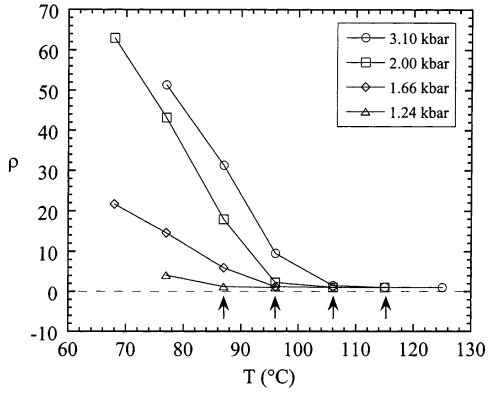

Figure 8. Temperature dependence of ρ, the scattering intensity at $q = 0.021$ nm^{-1} measured in the final time interval at each temperature step, $I_F(T)$, normalized by the measured intensity at $q = 0.021$ nm^{-1} in the final time interval of the last temperature of the dissolution experiment, $I_F(T_{last})$. The arrows indicate the temperature at which dissolution was obtained (the temperature which first leads to $\rho \approx 1$).

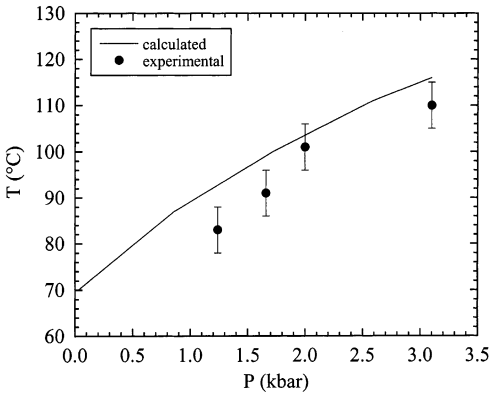

Figure 9. Comparison of the experimentally determined binodal temperature (solid circles) to the binodal temperature calculated from Flory−Huggins theory (curve) as a function of pressure for the B3 blend with no adjustable parameters.

in Figure 9 is remarkable, given the difficulty of attaining equilibrium in macroscopic samples of high molecular weight polymer blends and the fact that the agreement in Figure 9 is obtained without any adjustable parameters. The determination of χ in off-critical blends is usually subject to substantial errors (±20% or larger) due mainly to uncertainties in molecular weight and instrument calibration. These effects are not relevant to the present study because the same blend and instrument configuration used to determine χ was also used in the dissolution experiments. Additional complications in computing the binodal arise due to the composition dependence of χ that is found in many systems.[42−44] This is also not relevant for our system. The composition independence of χ (within experimental error) in PMB/PEB blends has been clearly established in several studies.[17−20,32,45,46] The effects of a subtle composition dependence of χ that might exist in our system is mitigated by our use of the same blend for determining the binodal and χ.

Conclusions

We began our study by determining the χ parameter of our PMB/PEB blend over a wide temperature and pressure range. We showed that χ, which is a nonlinear function of $1/T$ at low pressures, assumes the usually observed linear dependence on $1/T$ at elevated pressures

(above 2.5 kbar). The application of pressure thus leads to a simplification of thermodynamic properties of PMB/PEB blends. We show that the traditional cloud point method (using both neutrons and light) for estimating binodals would lead to errors in our system due to the presence of nucleation barriers. In contrast, we find that nucleation barriers are absent during dissolution of phase-separated structures. The phase boundary determined from the dissolution experiments is in quantitative agreement with predictions based on the Flory–Huggins theory.

Acknowledgment. We thank Boualem Hammouda for insightful suggestions and illuminating discussions on thermodynamics and phase transitions in polymers. We also thank Zhen-Gang Wang and John Prausnitz for educational discussions. This work is supported by National Science Foundation (Grant CTS-0196066). The SANS instrument is supported by Grant DMR-9986442 from the National Science Foundation to NIST.[48]

References and Notes

(1) Gunton, J. D.; San Miguel, M.; Sahani in *Phase Transitions;* Academic: New York, 1983; Vol. 8.
(2) Debenedetti, P. G. *Metastable Liquids Concepts and Principles*; Princeton University Press: Princeton, NJ, 1996.
(3) Strobl, G. *The Physics of Polymers Concepts for Understanding Their Structure and Behavior*; Springer-Verlag: New York, 1997.
(4) Balsara, N. P.; Lin, C. C.; Hammouda, B. *Phys. Rev. Lett.* **1996**, *77*, 3847.
(5) Lefebvre, A. A.; Lee, J. H.; Jeon, H. S.; Balsara, N. P. *J. Chem. Phys.* **1999**, *111*, 6082.
(6) Lefebvre, A. A.; Lee, J. H.; Balsara, N. P.; Hammouda, B. *J. Chem. Phys.* **2002**, *116*, 4777.
(7) Lefebvre, A. A.; Balsara, N. P.; Vaidyanathan, C. Manuscript in preparation.
(8) Wood, S. M.; Wang, Z. G. *J. Chem. Phys.* **2002**, *116*, 2289.
(9) Howland, R. G.; Wong, N. C.; Knobler, C. M. *J. Chem. Phys.* **1980**, *73*, 522.
(10) Shibayama, M.; Yang, H.; Stein, R. S.; Han, C. C. *Macromolecules* **1985**, *18*, 2179.
(11) Cumming, A.; Wiltzius, P.; Bates, F. S.; Rosedale, J. H. *Phys. Rev. A* **1992**, *45*, 885.
(12) Nakata, M.; Kawate, K. *Phys. Rev. Lett.* **1992**, *68*, 2176.
(13) Maurer, W. W.; Bates, F. S.; Lodge, T. P.; Almdal, K.; Mortensen, K. *J. Chem. Phys.* **1998**, *108*, 2989.
(14) He, M.; Liu, Y.; Feng, Y.; Jiang, M.; Han, C. C. *Macromolecules* **1991**, *24*, 464.
(15) Wong, N. C.; Knobler, C. M. *J. Chem. Phys.* **1978**, *69*, 725.
(16) Scheffold, F.; Eiser, E.; Budkowski, A.; Steiner, U.; Klein, J.; Fetters, L. J. *J. Chem. Phys.* **1996**, *104*, 8786.
(17) Lefebvre, A. A.; Lee, J. H.; Balsara, N. P.; Hammouda, B. *Macromolecules* **2000**, *33*, 7977.
(18) Balsara, N. P.; Lefebvre, A. A.; Lee, J. H.; Lin, C. C.; Hammouda, B. *AIChE J.* **1998**, *44*, 2515.
(19) Lefebvre, A. A.; Lee, J. H.; Balsara, N. P.; Hammouda, B.; Krishnamoorti, R.; Kumar, S. *Macromolecules* **1999**, *32*, 5460.
(20) Lefebvre, A. A.; Lee, J. H.; Balsara, N. P.; Hammouda, B. *J. Polym. Sci., Polym. Phys. Ed.* **2000**, *38*, 1926.
(21) Hammouda, B.; Balsara, N. P.; Lefebvre, A. A. *Macromolecules* **1997**, *30*, 5572.
(22) Staverman, A. J.; Van Saten, J. H. *Recl. Trav. Chim.* **1941**, *60*, 76.
(23) Huggins, M. L. *J. Phys. Chem.* **1942**, *46*, 151.
(24) Flory, P. J. *J. Chem. Phys.* **1942**, *10*, 51.
(25) The volume changes estimated from our experiments are sufficiently small, such that the change in ϕ is negligible.
(26) Krishnamoorti, R. Ph.D. Thesis, Princeton University, Princeton, NJ, 1994.
(27) Rodgers, P. A. *J. Appl. Polym. Sci.* **1993**, *48*, 1061.
(28) de Gennes, P. G. *Scaling Concepts in Polymer Physics;* Cornell University Press: Ithaca, NY, 1979.
(29) Balsara, N. P.; Jonnalagadda, S. V.; Lin, C. C.; Han, C. C.; Krishnamoorti, R. *J. Chem. Phys.* **1993**, *99*, 10011.
(30) Rachapudy, H.; Smith, G. G.; Raju, V. R.; Graessley, W. W. *J. Polym. Sci., Polym. Phys. Ed.* **1979**, *17*, 1211.
(31) This paper is the second paper of a series on nucleation in binary PMB/PEB blends. In the first paper (ref 6) the blends that were studied were called B1 and B2. Thus, we refer to this third blend as B3.
(32) Lin, C. C.; Jonnalagadda, S. V.; Balsara, N. P.; Han, C. C.; Krishnamoorti, R. *Macromolecules* **1996**, *29*, 661.
(33) Lefebvre, A. A. Ph.D. Thesis, University of California, Berkeley, CA, to be submitted.
(34) For the RPA fits of the SANS measurements obtained in the low-temperature and high-pressure corner of our experimental window [data at (68 °C, 2.59 kbar), (68 °C, 3.10 kbar), and (49 °C, 1.72 kbar)] only χ was allowed to float, and α was set equal to 0.90, which was the value of α in the neighborhood of these points. Floating both α and χ led to α values as low as 0.75 and correspondingly smaller χ values (lower by about 10% or less, relative to the values reported in Figures 2 and 3). The quality of the fits using χ as the only adjustable parameter and $\alpha = 0.9$ was as good as the fits where both χ and α were allowed to float. We thus used χ as the only adjustable parameter in the experimental window described above. The data presented in Figures 2 and 3 represent the simplest explanation for the measured SANS profiles. While there remains some possibility of obtaining large changes in statistical segment lengths in the low-temperature and high-pressure corner of our experimental window, the uncertainty in the χ parameters due to this is not significant. This is because χ is related to the extrapolated intercept $I(q\rightarrow 0)$, which, in the mean-field limit, is independent of the statistical segment lengths and α.
(35) Krishnamoorti, R.; Graessley, W. W.; Balsara, N. P.; Lohse, D. J. *Macromolecules* **1994**, *27*, 3073.
(36) Flory, P. J. *Principles of Polymer Chemistry*; Cornell University Press: Ithaca, NY, 1953.
(37) Balsara, N. P. In *Physical Properties of Polymers Handbook;* AIP Press: Woodbury, NY, 1996; Chapter 19, p 257.
(38) Freed, K. F.; Dudowicz, J. *Macromolecules* **1998**, *31*, 6681.
(39) Higgins, J. S.; Benoît H. C. *Polymers and Neutron Scattering*; Oxford University Press: New York, 1994.
(40) The sample was studied as a function of decreasing temperature from 144 to 49 °C using 20 °C steps; at each temperature the pressure was increased in approximately 0.86 kbar steps to a maximum pressure of 3.10 kbar.
(41) Because of a problem with the instrument configuration, we were unable to convert the data obtained from the dissolution experiment at 1.24 kbar to absolute intensities. Thus, the binodal temperature shown in Figure 12 is based on relative intensity changes in the SANS profiles.
(42) Han, C. C.; Bauer, B. J.; Clark, J. C.; Muroga, Y.; Matsushita, Y.; Okada, M.; Chang, Q.; Tran-cong, T.; Sanchez, I. *Polymer* **1988**, *29*, 2002.
(43) Bates, F. S.; Muthukumar, M.; Wignall, G. D.; Fetters, L. J. *J. Chem. Phys.* **1988**, *89*, 535.
(44) Krishnamoorti, R.; Graessley, W. W.; Balsara, N. P.; Lohse, D. J. *J. Chem. Phys.* **1994**, *100*, 3894.
(45) Crist, B. *Macromolecules* **1998**, *31*, 5853.
(46) Lin, C. C.; Jeon, H. S.; Balsara, N. P.; Hammouda, B. *J. Chem. Phys.* **1995**, *103*, 1957.
(47) Wang, Z. G., to be submitted.
(48) Identification of equipment and materials does not imply recommendation by the National Institute of Standards and Technology.
(49) Balsara, N. P.; Fetters, L. J.; Hadjichristidis, N.; Lohse, D. J.; Han, C. C.; Graessley, W. W.; Krishnamoorti, R. *Macromolecules* **1992**, *25*, 6137.

MA020552X